Channel-Level Event-Triggered Communication Scheme for Path Tracking Control of Autonomous Ground Vehicles With Distributed Sensors

Liqin Zhang, Manjiang Hu, Hui Zhang, Yougang Bian, Tran Anh-Tu Nguyen, Rongjun Ding

Channel-Level Event-Triggered Communication Scheme for Path Tracking Control of Autonomous Ground Vehicles With Distributed Sensors

Article *in* IEEE Transactions on Vehicular Technology · May 2023

DOI: 10.1109/TVT.2023.3274111

CITATION
1

READS
67

6 authors, including:

Zhang Liqin
Hunan University
4 PUBLICATIONS **11** CITATIONS
SEE PROFILE

Yougang Bian
Hunan University
74 PUBLICATIONS **1,358** CITATIONS
SEE PROFILE

Anh-Tu Nguyen
Université Polytechnique Hauts-de-France
140 PUBLICATIONS **2,084** CITATIONS
SEE PROFILE

Channel-Level Event-Triggered Communication Scheme for Path Tracking Control of Autonomous Ground Vehicles with Distributed Sensors

Liqin Zhang, Manjiang Hu, Hui Zhang, *Senior Member, IEEE,* Yougang Bian, *Member, IEEE,* Anh-Tu Nguyen, *Member, IEEE,* Rongjun Ding

***Abstract*—In this paper, a channel-level event-triggered communication scheme is investigated for path tracking control of autonomous ground vehicles via an in-vehicle network to ensure path tracking performance while reducing network resource utilization. First, a path tracking system is established considering the effect of norm bounded uncertainty on lateral vehicle dynamics, and a state feedback path tracking controller is designed within the Takagi–Sugeno fuzzy framework. Next, a decentralized event-triggered communication scheme is adopted between the sensors and controller, which makes it possible to save communication resources at the channel level. Finally, the results in the CarSim-Simulink joint-simulation environment show that the proposed controller can ensure a reliable path tracking performance in both lateral offset and heading error. At the same time, compared with the simple time-triggered scheme, the proposed method can effectively reduce the usage of communication resources by more than 80%.**

***Index Terms*—Autonomous ground vehicle, path tracking, decentralized control, event-triggered control, networked control system.**

I. Introduction

AUTONOMOUS ground vehicles (AGVs) have attracted much research attention and achieved fruitful results, especially in reducing traffic accidents caused by driver errors [1], [2] and improving traffic efficiency and the economy [3], [4]. As a fundamental problem, path tracking control of AGVs directly affects the driving safety and riding comfort [5], [6], so it has always become a hot topic; see [2], [7]–[10] and the references therein.

Different path tracking strategies have been proposed in existing studies to help AGVs track pre-defined reference trajectories smoothly and accurately, e.g., game theory-based control [8], [9], sliding mode control [10], [11], model predictive control (MPC) [2], [12]–[15], and fuzzy logic control [7], [16], [17]. Most of these works are based on models, either kinematic or dynamic, and the accuracy of the model is extremely crucial to controller performance. Nevertheless, since vehicle systems are complex and nonlinear [18], there are inevitable mismatches between the model and the real one. For example, linear tire cornering stiffness is often used in vehicle models [5], but its actual value has obvious nonlinear characteristics [8], [19], [20]. Moreover, there are some time-varying parameters, e.g., vehicle mass [17], [21], and longitudinal speed [2], [13], [22], [23]. All these uncertainties may introduce uncontrollable conditions for path tracking control [7], and make it a tough task [24]. To deal with the aforementioned uncertainties, the Takagi–Sugeno (T-S) fuzzy method [16], [17], [21], has been proved to be an effective way. It is worth noting that the fuzzy system and controller studied above usually share the same membership function and have limited flexibility.

As a typical decentralized system, the vehicle control system has different types of sensors, controllers, and actuators that are scattered throughout the vehicle due to functional requirements. Known as network nodes [25], these sensors, controllers, and actuators are physically connected via a controller area network (CAN) to form a networked control system (NCS) [26], [27], resulting in a lighter wiring harness [28]. As part of the network, different nodes collect information about the vehicle state, and share the information with each other via the network. Nevertheless, in response to recent advances in vehicle safety and performance, including autonomous driving, more and more information must be transmitted over the in-vehicle network, exacerbating the occupancy of in-vehicle network resources [29]. Unfortunately, a high network bandwidth occupation will lead to problems such as network delay and packet loss, which are random and cannot be ignored [30]. To this end, the delay and data dropout problem of CAN was modeled in [31], and the path tracking problem of AGVs under random network delay was investigated in [32], [33]. Further, to proactively solve the issue of occupancy of

This work was supported by the National Natural Science Foundation of China (Grants 52222216, 52172384 and 52002126), S&T Innovation Program of Hunan Province (Grant 2021RC3048), Hunan Provincial Natural Science Foundation of China (Grants 2021JJ40086 and 2021JJ40095), and the State Key Laboratory of Advanced Design and Manufacturing for Vehicle Body with 61775006. (*Corresponding author: Manjiang Hu.*)

Liqin Zhang is with the State Key Laboratory of Advanced Design and Manufacturing for Vehicle Body, College of Mechanical and Vehicle Engineering, Hunan University, Changsha 410082, China (e-mail: liqinzhang@hnu.edu.cn).

Manjiang Hu, Yougang Bian and Rongjun Ding are with the State Key Laboratory of Advanced Design and Manufacturing for Vehicle Body, College of Mechanical and Vehicle Engineering, Hunan University, Changsha 410082, China, and also with the Wuxi Intelligent Control Research Institute of Hunan University, Wuxi 214115, China (e-mail: manjiang_h@hnu.edu.cn; byg10@foxmail.com; dingrj@hnu.edu.cn).

Hui Zhang is with the Department of Transportation Science and Engineering, Beihang University, Beijing 100191, China (e-mail: huizhang285@gmail.com).

Anh-Tu Nguyen is with the Laboratory LAMIH UMR CNRS 8201, Université Polytechnique Hauts-de-France, 59313 Valenciennes, France (e-mail: nguyen.trananhtu@gmail.com).

limited network resources, an event-triggered communication mechanism was proposed as an alternative mechanism to remove the limitations of the traditional periodic one, see [34] and its references for details. The existing literature has yielded some interesting results for the event-triggered control problem of CAN-based in-vehicle network systems, e.g., active suspension systems [29], [35], path following systems [19], [23], and lateral dynamics control systems [36]. However, most of the studies above rely on a centralized event-triggered communication mechanism (CETCM), which requires the event generator to obtain all state information simultaneously. Consequently, for distributed sensor systems like vehicles, the CETCM is unsuitable due to the difficulty of measuring all state information with a single sensor simultaneously, or the cost is too high [29], [37], [38]. The decentralized event-triggered communication mechanism (DETCM) is a more feasible solution [38], [39]. In this case, each individual sensor determines whether to broadcast and transmit data to the network according to only locally available information, which can effectively save network bandwidth resources. In addition, it should be pointed out that the controller and actuators are usually directly connected point-to-point and the computational resources of the controller are much more affluent compared to the limited network resources. Therefore, a time-triggered communication mechanism (TTCM) would be more appropriate.

Based on the above analysis, this paper discusses the path tracking control problem of AGVs with distributed sensors via a decentralized event-triggered communication scheme. As shown in Fig. 1, there is a communication network between the sensors and controller, which in turn is directly connected to the actuator through a zero-order-holder (ZOH). Different system states are sampled by corresponding sensors at a fixed time interval, and the sampled state values that meet the triggering condition are sent to the controller through a CAN bus with DETCM. After receiving and storing the sampled state values sent by the sensors, the controller periodically calculates the control input according to these values with TTCM. With the co-design of the path tracking control and decentralized event-triggered communication scheme, network resources are saved while guaranteeing satisfactory path tracking performance.

The main contributions of this paper are summarized as follows.

1) By taking into account the distribution nature of state sensing and communication in CAN-based vehicle control systems, a DETCM is proposed for path tracking control of AGVs. Compared with [19], [23], this method removes the assumption of synchronous state component sensing, and thus enables event-triggered communication in each measuring channel for further communication resource saving in CAN.
2) A general T-S fuzzy lateral dynamics model is established considering the influence of norm bounded uncertainties in, e.g., vehicle mass, longitudinal speed, and tire cornering stiffness, and an imperfect premise matching (IPM) method is adopted to design the path tracking controller. Compared with [19], [23], the controller does not require the same premise variables as the T-S fuzzy system, allowing greater flexibility in design.
3) By analyzing typical vehicle test cycles and CAN-induced delay characteristics, an algorithm for determining the membership function parameter is proposed to ensure that the membership function design conditions always hold. Unlike [40], [41], the membership function parameter is directly given, which results in a lack of clear physical meaning.
4) The effectiveness of the proposed path tracking controller with the decentralized event-triggered communication scheme is validated in a high-fidelity CarSim-Simulink joint-simulation environment.

The paper is organized as follows. Section II formulates the problem. Section III presents the main results. Simulation results are given in Section IV. Finally, Section V concludes the paper.

Notation: The integers fields, positive integers fields, n-dimensional Euclidean space, and $n \times m$ real matrix are denoted by $\mathbb{N}$, $\mathbb{N}^+$, $\mathbb{R}^n$, and $\mathbb{R}^{n\times m}$, respectively. The superscript 'T' ('-1') is used to represent the transpose (inverse) of a matrix. The space of square-integrable vector functions over $[0,\infty)$ is denoted by $L_2[0,\infty)$, and for $w(t) \in L_2[0,\infty)$, its 2-norm is denoted by $\|w(t)\|_2 = \sqrt{\int_{t=0}^{\infty} |w(t)|^2 dt}$. The symbol I (0) represents the identity (zero) matrix of appropriate size. For any square matrix X, $X>0$ ($X<0$) indicates a positive (negative) definite matrix. The symbol '$*$' stands for matrix blocks that can be deduced by symmetry. The symbol $\mathrm{diag}(\ldots)$ stands for a block diagonal matrix. Matrices throughout the paper, if not explicitly stated, are assumed to have compatible dimensions.

II. System Modeling and Problem Formulation

A. Lateral vehicle dynamics with parameter uncertainties and path tracking model

A common two-degree-of-freedom vehicle model, as shown in the upper left corner of Fig.1, is used for path tracking controller design in this subsection. Assuming that the tire slip angle is small and the vehicle's longitudinal speed v_x is constant, the lateral vehicle dynamics can be expressed in the following form

$$\begin{bmatrix} \dot{v}_y \\ \dot{r} \end{bmatrix} = \begin{bmatrix} \frac{-2(C_f+C_r)}{mv_x} & \frac{2(bC_r-aC_f)}{mv_x} - v_x \\ \frac{2(bC_r-aC_f)}{I_z v_x} & \frac{-2\left(a^2C_f+b^2C_r\right)}{I_z v_x} \end{bmatrix} \begin{bmatrix} v_y \\ r \end{bmatrix} + \begin{bmatrix} \frac{2C_f}{m} \\ \frac{2aC_f}{I_z} \end{bmatrix} \delta, \tag{1}$$

where the symbols are given in Table I.

Nevertheless, the cornering stiffness of a tire is not constant due to the nonlinear relationship between the tire lateral force and its slip angle [31]. Not only that, but different driving conditions will affect it, including tire slip angle, temperature, and many other factors [17]. Therefore, it is necessary to consider the change of the tire cornering stiffness. By introducing the uncertain cornering stiffness terms ΔC_f and ΔC_r, the tire cornering stiffness in (1) can be further expressed as [42]

$$C_i = C_{0i} + \Delta C_i \zeta_i(t), i \in \{f, r\}, \tag{2}$$

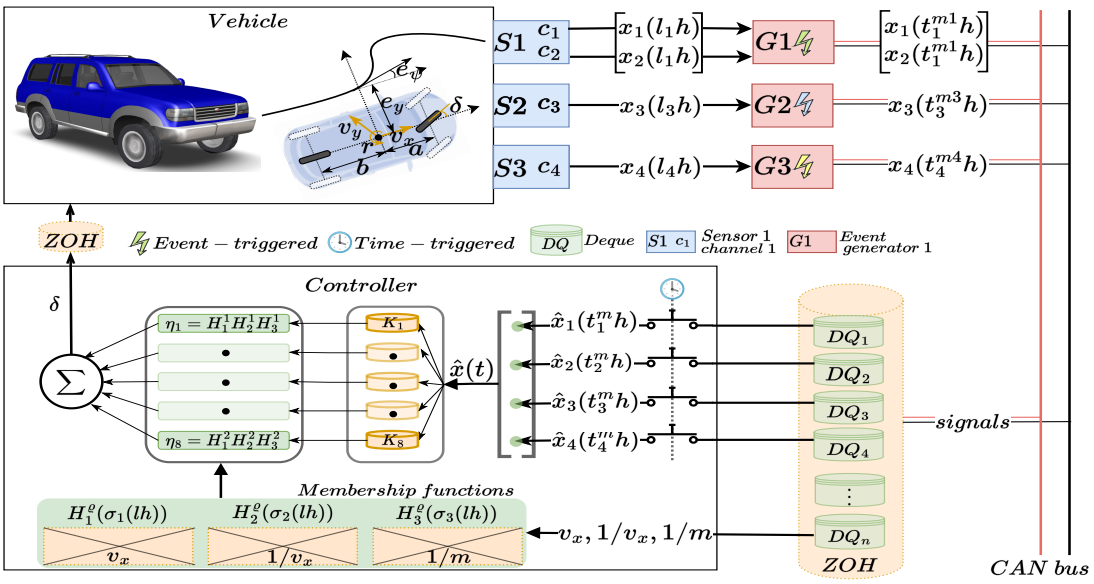

Fig. 1. A decentralized event-triggered communication scheme for AGVs with distributed sensors via an in-vehicle network.

TABLE I
NOMENCLATURE

Symbol	Description
m	vehicle total mass
I_z	yaw inertia around CG
C_f/C_r	front/rear tire cornering stiffness
C_{0f}/C_{0r}	normal value of C_f/C_r
a/b	distance from CG to the front/rear axle
v_x/v_y	longitudinal/lateral speed
r	yaw rate
δ	front wheel steering angle

CG: center of gravity

with $C_{0i} = \left(\overline{C}_i + \underline{C}_i\right)/2$, where $\overline{C}_i$ and $\underline{C}_i$ are the maximum and minimum values of C_i, respectively. ζ_i indicates an unknown time-varying parameter satisfying $|\zeta_i| \leq 1$, and the uncertain cornering stiffness can be represented by $\Delta C_i = \left(\overline{C}_i - \underline{C}_i\right)/2$.

Denote by e_y the lateral offset from the center of gravity (CG) to the closest point on the desired path s, and by e_ψ the heading error between the desired heading angle ψ_d and the actual one ψ, similar to [32], then the path tracking model of the AGV can be expressed as

$$\dot{e}_y = v_x e_\psi - v_y, \dot{e}_\psi = v_x \rho(s) - r, \tag{3}$$

where $\rho(s)$ is the road curvature along the desired path. In general, the lateral offset e_y and heading error e_ψ need to be as small as possible.

Denote $x(t) \triangleq [e_y, e_\psi, v_y, r]^{\mathrm{T}}$ as the state vector, $u(t) \triangleq \delta$ as the control input, and $\omega(t) \triangleq \rho(s)$ as the external disturbance. By using (1)-(3), the system model can be expressed in the following matrix form

$$\begin{aligned}\dot{x}(t) =& Ax(t) + Bu(t) + B_1\omega(t)\\ =& (A_0 + \Delta A)\, x(t) + (B_0 + \Delta B)\, u(t) + B_1\omega(t)\end{aligned} \tag{4}$$

where

$$A_0 = \begin{bmatrix} 0 & v_x & 1 & 0 \\ 0 & 0 & 0 & 1 \\ 0 & 0 & \frac{-2(C_f+C_r)}{mv_x} & \frac{2(bC_r-aC_f)}{mv_x} - v_x \\ 0 & 0 & \frac{2(bC_r-aC_f)}{I_z v_x} & \frac{-2\left(a^2C_f+b^2C_r\right)}{I_z v_x} \end{bmatrix},$$

$B_0 = \begin{bmatrix} 0 & 0 & \frac{2C_f}{m} & \frac{2aC_f}{I_z} \end{bmatrix}^{\mathrm{T}}$, and $B_1 = \begin{bmatrix} 0 & -v_x & 0 & 0 \end{bmatrix}^{\mathrm{T}}$.

In addition, the matrices ΔA and ΔB are norm-bounded uncertainties caused by the uncertain cornering stiffness ΔC_f and ΔC_r. According to (1) and (2), we have

$$\begin{bmatrix} \Delta A & \Delta B \end{bmatrix} = EF \begin{bmatrix} G_1 & G_2 \end{bmatrix}, \tag{5}$$

where

$$E = \begin{bmatrix} 0 & 0 & \frac{-2\Delta C_r}{mv_x} & \frac{2b\Delta C_r}{I_z v_x} \\ 0 & 0 & \frac{-2\Delta C_f}{mv_x} & \frac{-2a\Delta C_f}{I_z v_x} \end{bmatrix}^{\mathrm{T}}, G_1 = \begin{bmatrix} 0 & 0 & 1 & -b \\ 0 & 0 & 1 & a \end{bmatrix},$$

$F(t) = \mathrm{diag}\left(\zeta_r(t), \zeta_f(t)\right)$, and $G_2 = \begin{bmatrix} 0 & -v_x \end{bmatrix}^{\mathrm{T}}$.

Remark 1. To reduce the complexity of the problem, it is reasonable to assume that the unknown time-varying parameters $\zeta_f(t) = \zeta_r(t) = \zeta(t)$ because the road conditions are usually uniform to both the front and rear wheels [31]. In this case, the matrix $F(t)$ can be written as $F(t) = \zeta(t) \cdot \mathrm{diag}(1, 1)$.

B. T-S fuzzification of the vehicle model

It is noted that the longitudinal vehicle velocity generally varies due to the exterior driving environment or other reasons in practical applications. With the velocity changing, system (4) will be time-varying due to the existence of the term v_x. In addition, vehicle mass m and yaw inertia I_z vary with the number of passengers or vehicle load, which also causes system time-varying. In this subsection, the T-S fuzzy modeling approach will be adopted to deal with the time-varying problem caused by the above parameter changes [43].

Without loss of generality, the varying longitudinal vehicle velocity v_x is bounded in the range $[\underline{v}_x, \overline{v}_x]$ with $\underline{v}_x, \overline{v}_x > 0$,

and the vehicle mass m varies in the interval $[\underline{m}, \overline{m}]$. Define $\sigma_1(t) \triangleq v_x, \sigma_2(t) \triangleq \frac{1}{v_x}$, and $\sigma_3(t) \triangleq \frac{1}{m}$ as the premise variables, the uncertain term can be presented as follows

$$\sigma_k(t) = H_{k,1}(\sigma_k(t))\overline{\sigma}_k + H_{k,2}(\sigma_k(t))\underline{\sigma}_k, k \in \{1,2,3\}, \quad (6)$$

where the overline $\overline{\bullet}$ and the underline $\underline{\bullet}$ denote the maximum and minimum values of $\bullet$, respectively. The membership functions $H_{k,1}(\sigma_k(t))$ and $H_{k,2}(\sigma_k(t))$ in (6) satisfy the following relationship

$$H_{k,1}(\sigma_k(t)) = \frac{\overline{\sigma}_k - \sigma_k(t)}{\overline{\sigma}_k - \underline{\sigma}_k}, H_{k,2}(\sigma_k(t)) = \frac{\sigma_k(t) - \underline{\sigma}_k}{\overline{\sigma}_k - \underline{\sigma}_k}. \quad (7)$$

It is easy to find that $H_{k,1}(\sigma_k(t)) + H_{k,2}(\sigma_k(t)) \equiv 1$.

Combining the above analysis, system (4) with time-varying parameter $\sigma_k(t)$ can be formulated by the following IF-THEN rules based on the T-S fuzzy modeling method [44]:

Model Rule j: IF $\sigma_1(t)$ is $H_{1,\varrho}(\sigma_1(t))$, $\sigma_2(t)$ is $H_{2,\varrho}(\sigma_2(t))$, and $\sigma_3(t)$ is $H_{3,\varrho}(\sigma_3(t))$, THEN

$$\begin{aligned}\dot{x}(t) =& A_j\left(\sigma_1(t), \sigma_2(t), \sigma_3(t)\right) + B_j\left(\sigma_3(t)\right)u(t) \\ &+ B_{1j}\left(\sigma_1(t)\right)\omega(t)\end{aligned}, \quad (8)$$

where $\varrho \in \{1,2\}, j \in \{1,2,\ldots,8\}$, and the matrices A_j, B_j, and B_{1j} can be obtained by replacing $\sigma_k(t)$ with the maximum value $\overline{\sigma}_k$ or the minimum value $\underline{\sigma}_k$ in system model (4), respectively.

For convenience, fuzzy system (8) is further expressed in the following concise form

$$\dot{x}(t) = \sum_{j=1}^{8} \eta_j(\sigma(t))\left[A_j x(t) + B_j u(t) + B_{1j}\omega(t)\right] \quad (9)$$

where the membership factor $\eta_j(\sigma(t))$ is nonnegative and $\sum_{j=1}^{8} \eta_j(\sigma(t)) = 1$. For brevity, denote $\eta_j \triangleq \eta_j(\sigma(t))$, then it can be specifically defined as follows

$$\begin{aligned}\eta_1 &= H_{1,1}(\sigma_1(t))H_{2,1}(\sigma_2(t))H_{3,1}(\sigma_3(t)) \\ \eta_2 &= H_{1,1}(\sigma_1(t))H_{2,1}(\sigma_2(t))H_{3,2}(\sigma_3(t)) \\ &\ldots \qquad\qquad \ldots \qquad\qquad \ldots \\ \eta_8 &= H_{1,2}(\sigma_1(t))H_{2,2}(\sigma_2(t))H_{3,2}(\sigma_3(t))\end{aligned}. \quad (10)$$

Remark 2. The changes in vehicle mass m and yaw inertia I_z often exist at the same time. To reduce the complexity of the T-S fuzzy system, in this study, we assume that the value of I_z changes simultaneously with m, that is, when the vehicle mass is at its maximum value, the yaw inertia also takes the maximum value, and vice versa.

C. Decentralized event-triggered communication mechanism design

In this subsection, a DETCM is proposed to address the limitation of the centralized one by designing individual triggering conditions for each sensor. Specifically, each system state component $x_n(t), n \in \mathbb{N}^+$, is measured by sensing unit Sn at a constant sampling interval h, and the sampled system state at time $l_n h$ is denoted as $x_n(l_n h), l_n \in \mathbb{N}$. And then, event generator Gn determines whether to broadcast and transmit the current sampled data $x_n(l_n h)$, through a unique frame ID, by judging whether it meets the triggering condition. If it does, record the current sampled data as $x_n(t_n^m h)$, where $t_n^m h$ is the event-triggering instant of Gn, $t_n^m \in \mathbb{N}$.

Remark 3. DETCM described above is a general mechanism for distributed sensing systems. Specific to this study, since the lateral offset e_y and heading error e_ψ are generated by the same network node, it is natural to encapsulate them in the same data frame and send together. In particular, as depicted in Fig. 1, the event generator $G1$ makes trigger judgments according to the sampling values of the two measurement channels, i.e., c_1 and c_2, of the sensing unit $S1$. A CAN data frame, containing the current e_y and e_ψ, will be sent to the network if the trigger condition is met; otherwise, it will not. As a result, the timestamps of their samples are the same in this case, which we denote by t_1^{m1} in Fig. 1. Similarly, in the following, we will provide a general derivation of distributed sensing systems, based on which we will specify the path tracking problem studied in this study.

A memory stack is allocated for each state component, and once a frame update for Sn is received, its value is pushed to the top of the corresponding stack, which is periodically read by the controller. According to the CAN communication protocol, e.g., ISO 11898, only one network node can send a frame at the same time. In addition, the priority of sending is determined by the ID of the frame. The smaller the ID, the higher the priority. For those frames that fail to compete, they will be waiting for the frames with higher priority to be sent before sending. Therefore, there will be an inevitable time delay.

Considering the limited bandwidth of the CAN network, a DETCM is introduced to reduce the communication burden without sacrificing too much system performance. The event generator Gn is employed to determine the next triggering instant for sensor Sn with the following triggering rule

$$t_n^{m+1} = t_n^m + \min\left\{ l_n \,\middle|\, \begin{array}{l} e_n^{\mathrm{T}}\left(t_n^m h + l_n h\right)\Phi_n e_n\left(t_n^m h + l_n h\right) \\ \geq \epsilon_n(t) x_n^{\mathrm{T}}\left(t_n^m h\right)\Phi_n x_n\left(t_n^m h\right) \end{array} \right\} \quad (11)$$

where $e_n\left(t_n^m h + l_n h\right)$ is the error between the latest transmitted state $x_n\left(t_n^m h\right)$ and the current sampled state $x_n\left(t_n^m h + l_n h\right)$, i.e.,

$$e_n(t_n^m h + l_n h) = x_n\left(t_n^m h\right) - x_n\left(t_n^m h + l_n h\right). \quad (12)$$

The weighting matrix Φ_n is a positive definite matrix of appropriate size to be designed. Considering all states of the system, define an aggregated weight matrix Φ as

$$\Phi = \mathrm{diag}(\Phi_1, \Phi_2, \ldots, \Phi_n). \quad (13)$$

Remark 4. The positive weight matrix Φ to be designed in (13) is a block diagonal matrix, which is the main difference between the DETCM and the centralized ones. In this case, special treatment is required in the solution process, which will be covered later in *Remark* 10. Specific to system (4), there are n equals 3, $\Phi_1 \in \mathbb{R}^2$, Φ_2 and Φ_3 are positive constants.

In addition, the event-triggering threshold $\epsilon_n(t)$ is calculated with the following update rule

$$\dot{\epsilon}_n(t) = \epsilon_n^{-1}(t)\left[\epsilon_n^{-1}(t) - \epsilon_0\right] e_n^{\mathrm{T}}\left(t_n^m h + l_n h\right)\Phi_n e_n\left(t_n^m h + l_n h\right), \quad (14)$$

where $\epsilon_0 > 0$ is a given initial scalar parameter.

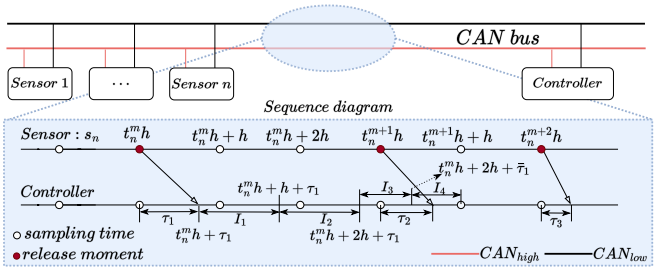

Fig. 2. An example of a CAN signal transmission sequence diagram.

Remark 5. Each event generator determines whether or not to transmit the current sampled data based solely on locally available information, which makes it possible to improve the communication bandwidth occupation from the channel level. When condition (11) is satisfied, the sensor will apply for data transmission. At this time, if the bus is free and there is no higher-priority frame competition, the sampled status data will be broadcast. Otherwise, it will wait until the higher-priority frame is sent and the bus is free before sending. When condition (11) is not met, the current sampled data will be discarded directly. Therefore, the number of sample data transfers can be reduced.

D. Controller design of the networked control system

The broadcast feature of CAN communication ensures that once a network node sends a message to the bus, the other network nodes will immediately start receiving it. However, it will take some time for the message to be transmitted over the network. For example, the theoretical transmission time is approximately 216us for a 108-bit standard data frame on a high-speed CAN network with a communication speed of 500kbps. Furthermore, due to bus occupancy and the necessary read/write operations of the microprogrammed control unit [30], the complete receipt of the message by a specific network node tends to lag further. Therefore, there is inevitably a network-induced delay in the process of network information transmission, as shown in Fig. 2 [27], which will deteriorate the control performance of the NCS.

Without losing generality, define the moment when the controller receives the message sent by sensor Sn as

$$T_n^m = t_n^m h + \tau_n^m,$$

where τ_n^m is the network-induced delay.

Therefore, the system state received by the controller can be expressed as

$$\hat{x}_n(t_n) = x_n(t_n^m h), t_n \in \Omega \triangleq [t_n^m h + \tau_n^m, t_n^{m+1} h + \tau_n^{m+1}), \tag{15}$$

where τ_n^m $(m \in \mathbb{N}^+)$ is the norm bounded delay that satisfies $\underline{\tau} \leq \tau_n^m \leq \overline{\tau}$.

Remark 6. For the same electrical environment, to simplify the problem, we consider that the upper and lower bounds of network-induced delay for different network nodes are the same.

Further, similar to [27], we consider the following two cases for time interval Ω.

Case 1: If $t_n^m h + h + \overline{\tau} \geq t_n^{m+1} h + \tau_n^{m+1}$, define a function $\tau_n(t_n)$ as

$$\tau_n(t_n) = t_n - t_n^m h, \quad t_n \in \Omega, \tag{16}$$

where $\tau_n^m \leq \tau_n(t_n) \leq (t_n^{m+1} - t_n^m)h\tau_n^{m+1} \leq h\overline{\tau}$.

Case 2: If $t_n^m h + h + \overline{\tau} < t_n^{m+1} h + \tau_n^{m+1}$, since $t_n^m < \overline{\tau}$, it can be easily checked that there exists a positive integer d_M such that

$$t_n^m h + d_M h + \overline{\tau} < t_n^{m+1} h + \tau_n^{m+1} \leq t_n^m h + d_M h + h + \overline{\tau}$$

for the time interval $[t_n^m h + \tau_n^m, t_n^m h + h + \overline{\tau}) \cup [t_n^m h + \Delta^+ h + \tau_n^m, t_n^m h + \Delta^+ h + h + \overline{\tau})$ with $\Delta^+ = 1, 2, \ldots, d_M$, and $d_M = \min\left(l_n | t_n^m h + \tau_n^m + l_n h \geq t_n^{m+1} h + \tau_n^{m+1}\right)$.

Therefore, the time interval Ω can be divided into the following subintervals

$$\Omega = \cup_{\Delta=0}^{d_M} \Omega_\Delta, \quad \Delta = 0, 1, \ldots, d_M, \tag{17}$$

where

$$\begin{cases} \Omega_0 = [t_n^m h + \tau_n^m, t_n^m h + h + \overline{\tau}) \\ \Omega_{\Delta'} = [t_n^m h + \Delta' h + \tau_n^m, t_n^m h + \Delta' h + h + \overline{\tau}) \\ \Omega_{d_M} = [t_n^m h + d_M h + \overline{\tau}, t_n^{m+1} h + \tau_n^{m+1}) \end{cases}$$

with $\Delta' = 1, 2, \ldots, d_M - 1$.

Define the following piecewise function

$$\tau_n(t_n) = \begin{cases} t_n - t_n^m h, & t_n \in \Omega_0 \\ t_n - t_n^m h - \Delta' h, & t_n \in \Omega_{\Delta'} \\ t_n - t_n^m h - d_M h, & t_n \in \Omega_{d_M} \end{cases}. \tag{18}$$

Then it can be obtained that

$$\begin{cases} \tau_n^m \leq \tau_n(t_n) \leq h + \overline{\tau}, & t_n \in \Omega_0 \\ \tau_n^m \leq \overline{\tau} \leq \tau_n(t_n) \leq h + \overline{\tau}, & t_n \in \Omega_{\Delta'} \\ \tau_n^m \leq \overline{\tau} \leq \tau_n(t_n) \leq h + \overline{\tau}, & t_n \in \Omega_{d_M} \end{cases}.$$

Therefore, we have

$$\underline{\tau} \triangleq \tau_m \leq \tau_n^m \leq \tau_n(t_n) \leq (h + \overline{\tau}) \triangleq \tau_M, \quad t_n \in \Omega. \tag{19}$$

Based on the analysis above, for time interval Ω, in Case 1, define $e_n(t_n) = 0$; in Case 2, define

$$e_n(t_n) = \begin{cases} 0, & t_n \in \Omega_0 \\ x_n(t_n^m h) - x_n(t_n^m h - \Delta' h), & t_n \in \Omega_{\Delta'} \\ x_n(t_n^m h) - x_n(t_n^m h - d_M h), & t_n \in \Omega_{d_M} \end{cases}.$$

Then according to (16) and (18), the following expression holds

$$e_n(t_n) = x_n(t_n^m h) - x_n(t_n - \tau(t_n)), \quad t_n \in \Omega. \tag{20}$$

Substituting (20) into (15), one has

$$\hat{x}_n(t_n) = e_n(t_n) + x_n(t_n - \tau_n(t_n)), \quad t_n \in \Omega. \tag{21}$$

It is assumed that system (9) is controlled over a CAN communication network with a state feedback controller. Due to the existence of communication network delays, it is unreasonable to assume that the controller shares the same premise

variables with the system. Therefore, a fuzzy controller is designed as follows by using the IPM method [40], [41]:

Controller Rule r: IF $\sigma_1(lh)$ is $H_{1,\varrho}(\sigma_1(lh))$, $\sigma_2(lh)$ is $H_{2,\varrho}(\sigma_2(lh))$, and $\sigma_3(lh)$ is $H_{3,\varrho}(\sigma_3(lh))$, THEN

$$u(t) = K_r\hat{x}(t), \quad t \in [lh, (l+1)h), \tag{22}$$

where $r \in \{1, 2, \ldots, 8\}$, $\hat{x}(t) \triangleq [\hat{x}_1(t_1^m h), \hat{x}_2(t_2^m h), \hat{x}_3(t_3^m h), \hat{x}_4(t_4^m h)]^{\mathrm{T}}$ is the system state vector reassembled from the latest available data received by the controller, and K_r is the controller gain to be designed.

Remark 7. The vehicle's lateral velocity is often not directly measurable or costly to measure directly. In this case, state estimation methods such as the Kalman filter and its extended form can be applied; see [45]–[47] and the reference therein.

Let $e(t) \triangleq [e_1(t_1), e_2(t_2), e_3(t_3), e_4(t_4)]^{\mathrm{T}}$ and $x(t-\tau(t)) \triangleq [x_1(t_1-\tau_1(t_1)), \ldots, x_4(t_4-\tau_4(t_4))]^{\mathrm{T}}$, where $t_n \in \Omega$. According to (21) and (22), the fuzzy controller can be expressed as follows by employing fuzzy reasoning

$$u(t) = \sum_{r=1}^{8} \mu_r(\sigma(lh))K_r\left[e(t) + x(t-\tau(t))\right], \tag{23}$$

where the membership factors $\mu_r(\sigma(lh))$, shortened as $\mu_r \triangleq \mu_r(\sigma(lh))$, are defined in (10) with η_j, and $\sigma(t)$ replaced by μ_r and $\sigma(lh)$, respectively.

Combining (9) and (23), it yields the closed-loop fuzzy system as follows

$$\begin{aligned}\dot{x}(t) = &\sum_{j=1}^{8}\sum_{r=1}^{8} \eta_j\mu_r\left[A_{jr}x(t) + B_jK_rx(t-\tau(t))\right.\\ &\left.+B_jK_re(t) + B_{1j}\omega(t)\right]\end{aligned}. \tag{24}$$

E. Problem formulation

In the following design process, we aim to improve the following performance of the AGV while maintaining its lateral stability. Therefore, the controlled output vector is chosen as follows

$$z(t) = Cx(t), \tag{25}$$

where $C = \mathrm{diag}(q_1,q_2,q_3,q_4)$, q_n is the weighting coefficient reflecting the degree of importance, and $C = I$.

We can now formulate the main problem of this study as designing an appropriate event-triggered fuzzy controller in form (23) using the DETCM (11) so that

1) closed-loop system (24) with a time-varying parameter is asymptotically stable when the external disturbance $\omega(t) \equiv 0$;
2) under zero initial conditions, the effect from external input $\omega(t)$ to signal $z(t)$ satisfies

$$\left\|z(t)\right\|_2 < \gamma\left\|\omega(t)\right\|_2 \tag{26}$$

for all nonzero $\omega(t) \in L_2[0,\infty)$ with an H_∞ performance $\gamma > 0$.

The following lemmas will be used later for the proof of the main results.

Lemma 1. *[23] For given positive scalars $0 \le \tau_m \le \tau_M$, $\epsilon_0 > 0$ and $\gamma > 0$, closed-loop system* (24) *is asymptotically stable and satisfies desired condition* (26) *if there exist positive definite matrices P, Q_1, Q_2, R_1, R_2, Φ, and feedback gains K_r such that ($j, r = 1, 2, \ldots, 8$)*

$$\Psi_{jr} = \begin{bmatrix}\Psi_{jr}^{11} & \Psi_{jr}^{12} & \Psi_{jr}^{13}\\ * & \Psi^{22} & \Psi_{jr}^{23}\\ * & * & \Psi^{33}\end{bmatrix} < 0, \tag{27}$$

where

$$\Psi_{jr}^{11} = \begin{bmatrix}\Sigma_{jr}^{11} & PB_jK_r & R_1\\ * & \Sigma^{22} & R_2\\ * & * & \Sigma^{33}\end{bmatrix}, \Psi_{jr}^{12} = \begin{bmatrix}0 & PB_jK_r & PB_{1j}\\ R_2 & \Phi & 0\\ 0 & 0 & 0\end{bmatrix},$$
$$\Sigma_{jr}^{11} = PA_j + A_j^{\mathrm{T}}P + Q_1 + Q_2 - R_1, \Sigma^{22} = -2R_2 + \Phi,$$
$$\Sigma^{33} = -Q_1 - R_1 - R_2, \Psi_{jr}^{13} = \begin{bmatrix}\tau_mA_j^{\mathrm{T}} & \Delta\tau A_j^{\mathrm{T}} & C^{\mathrm{T}}\\ \tau_mK_r^{\mathrm{T}}B_j^{\mathrm{T}} & \Delta\tau K_r^{\mathrm{T}}B_j^{\mathrm{T}} & 0\\ 0 & 0 & 0\end{bmatrix},$$
$$\Psi^{22} = \mathrm{diag}\left(-Q_2 - R_2, (1-\epsilon_0)\,\Phi, -\gamma^2 I\right),$$
$$\Psi_{jr}^{23} = \begin{bmatrix}0 & 0 & 0\\ \tau_mK_r^{\mathrm{T}}B_j^{\mathrm{T}} & \Delta\tau K_r^{\mathrm{T}}B_j^{\mathrm{T}} & 0\\ \tau_mB_{1j}^{\mathrm{T}} & \Delta\tau B_{1j}^{\mathrm{T}} & 0\end{bmatrix},$$
$$\Psi^{33} = \mathrm{diag}\left(-R_1^{-1}, -R_2^{-1}, -I\right), \Delta\tau = \tau_M - \tau_m.$$

Lemma 2. *[48] For given matrices $\Theta = \Theta^{\mathrm{T}}$, Υ, and Γ of appropriate dimensions, and $F(t)$ satisfying $F^{\mathrm{T}}(t)F(t) \le I$, the following inequality*

$$\Theta + \Upsilon F(t)\Gamma + (\Upsilon F(t)\Gamma)^{\mathrm{T}} < 0$$

holds if and only if there exists a scalar $\varepsilon > 0$ such that

$$\begin{bmatrix}\Theta & \Upsilon & \varepsilon\Gamma^{\mathrm{T}}\\ * & -\varepsilon I & 0\\ * & * & -\varepsilon I\end{bmatrix} < 0.$$

Lemma 3. *[31] For matrices X, $W > 0$, and scalar $\kappa > 0$, the following conditions are equivalent*

(1) $(W - \kappa^{-1}X)^{\mathrm{T}}W^{-1}(W - \kappa^{-1}X) \ge 0$,
(2) $\kappa^2 W - 2\kappa X \ge -XW^{-1}X$.

III. Main results

The following section derives a sufficient condition that ensures the asymptotic stability of closed-loop system (24) with DETCM.

Theorem 1. For the given constants γ, h, ϵ_0, τ_m, τ_M $(0 < \tau_m \le \tau_M)$, and the membership functions satisfying $\mu_r - \lambda_r\eta_r > 0$ $(0 < \lambda_r \le 1)$, closed-loop system (24) is asymptotically stable with control gains K_r if there exit symmetric positive definite matrices P, Q_1, Q_2, R_1, R_2, Φ, and arbitrary positive definite matrices Λ_j of appropriate dimensions such that the following matrix inequality conditions hold for any $j, r = 1, 2, \ldots, 8$:

$$\Xi_{jr} - \Lambda_j < 0, \tag{28}$$

$$\lambda_j\Xi_{jj} + (1-\lambda_j)\Lambda_j < 0, \tag{29}$$

$$\lambda_r\Xi_{jr} + \lambda_j\Xi_{rj} + (1-\lambda_r)\Lambda_j + (1-\lambda_j)\Lambda_r < 0, j < r, \tag{30}$$

where

$$\Xi_{jr} = \begin{bmatrix}\Xi_{jr}^{11} & \Xi_{jr}^{12}\\ * & \Xi^{22}\end{bmatrix}, \Xi_{jr}^{11} = \Psi_{jr}^{0}, \Xi^{22} = \mathrm{diag}\left(-\varepsilon_1 I, -\varepsilon_1 I\right),$$

$\Xi_{jr}^{12} = \begin{bmatrix} E_j^{\mathrm{T}}P & 0 & 0\,0 & 0 & 0\,\tau_m E_j^{\mathrm{T}} & \Delta\tau E_j^{\mathrm{T}} & 0 \\ \varepsilon_1 G_1 & \varepsilon_1 G_2 K_r & 0\,0 & \varepsilon_1 G_2 K_r & 0 & 0 & 0 \end{bmatrix}^{\mathrm{T}}$, and Ψ_{jr}^0 can be obtained from (27) by replacing A_j and B_j with A_{0j} and B_{0j}, respectively.

Proof. Based on **Lemma 1**, by recalling the uncertainties defined in (5), we obtain that

$$\Psi_{jr} = \Psi_{jr}^0 + WF\Pi + (WF\Pi)^{\mathrm{T}} < 0, \tag{31}$$

where $W^{\mathrm{T}} \triangleq [E_j^{\mathrm{T}}P,0,0,0,0,0,\tau_m E_j^{\mathrm{T}}, \Delta\tau E_j^{\mathrm{T}},0]$, $\Pi \triangleq [G_1,G_2K,0,0,G_2K,0,0,0,0]$, and Ψ_{jr}^0 can be obtained from (27) by replacing A_j and B_j with A_{0j} and B_{0j}, respectively.

By using **Lemma 2**, inequality (31) is equivalent to

$$\Xi_{jr} = \begin{bmatrix} \Psi_{jr}^0 & W & \varepsilon_1\Pi^{\mathrm{T}} \\ * & -\varepsilon_1 I & 0 \\ * & * & -\varepsilon_1 I \end{bmatrix} < 0. \tag{32}$$

Then, for vector $\xi(t)$ with appropriate dimensions, we have

$$\sum_{j=1}^{8}\sum_{r=1}^{8} \eta_j\mu_r\xi^{\mathrm{T}}(t)\Xi_{jr}\xi(t) < 0. \tag{33}$$

Consider a slack matrix

$$\sum_{j=1}^{8}\sum_{r=1}^{8} \eta_j(\mu_r - \eta_r)\Lambda_j = \sum_{j=1}^{8}\eta_j(\sum_{r=1}^{8}\eta_r - \sum_{r=1}^{8}\mu_r)\Lambda_j \equiv 0$$

as described in [40]. Substituting these terms into (33) yields

$$\begin{aligned} &\textstyle\sum_{j=1}^{8}\sum_{r=1}^{8}\eta_j\mu_r\xi^{\mathrm{T}}(t)\Xi_{jr}\xi(t) = \sum_{j=1}^{8}\eta_j^2\xi^{\mathrm{T}}(t)[\lambda_j\Xi_{jj} \\ &+(1-\lambda_j)\Lambda_j]\xi(t) + \textstyle\sum_{j=1}^{8}\sum_{j<r}^{8}\eta_j\eta_r\xi^{\mathrm{T}}(t)[\lambda_r\Xi_{jr} + \lambda_j\Xi_{rj} \\ &+(1-\lambda_r)\Lambda_j + (1-\lambda_j)\Lambda_r]\xi(t) + \textstyle\sum_{j=1}^{8}\sum_{r=1}^{8}\eta_j(\mu_r \\ &-\lambda_r\eta_r)\xi^{\mathrm{T}}(t)[\Xi_{jr} - \Lambda_j]\xi(t). \end{aligned} \tag{34}$$

Then if $\mu_r - \lambda_r\eta_r > 0$ and (28)-(30) hold for all $r = 1,2,\ldots,8$, desired condition (26) can be guaranteed. This completes the proof. ■

Remark 8. Although the introduction of membership function design condition $\mu_r - \lambda_r\eta_r > 0$ leads to conservative stability analysis results [40], more relaxed stability analysis and controller synthesis results can be developed [41], especially for NCSs with communication network delays.

Remark 9. In this study, due to network-induced delay, the fuzzy controller does not share the same premise variables as the T-S fuzzy mode, i.e., $\mu_r \neq \eta_r$, so the IPM method is used to derive **Theorem 1**. If $\mu_r = \eta_r$ in (24), we can use similar perfect premise matching methods, e.g., the parallel distribution compensation (PDC) technology [19], [23], to get the corresponding results. Therefore, the PDC technique can be regarded as a special case of the proposed method.

Although **Theorem 1** can guarantee the stability and the performance of closed-loop system (24), the controller gain is coupled with unknown matrix variables, and matrix inequalities (28)-(30) are non-convex. On this basis, controller gains in form (22) can be obtained in the following theorem.

Theorem 2. For the given constants γ, h, ϵ_0, τ_m, τ_M $(0 < \tau_m \leq \tau_M)$, and the membership functions satisfying $\mu_r - \lambda_r\eta_r > 0$ $(0 < \lambda_r \leq 1)$, closed-loop system (24) is asymptotically stable with control gains K_r if there exist symmetric positive definite matrices $\widetilde{P}$, $\widetilde{\Phi}$, $\widetilde{Q}_1$, $\widetilde{Q}_2$, $\widetilde{R}_1$, $\widetilde{R}_2$, and arbitrary positive definite matrices $\widetilde{\Lambda}_j$ of appropriate dimensions such that the following linear matrix inequality conditions hold for any $j,r = 1,2,\ldots,8$:

$$\widetilde{\Xi}_{jr} - \widetilde{\Lambda}_j < 0, \tag{35}$$

$$\lambda_j\widetilde{\Xi}_{jj} + (1-\lambda_j)\widetilde{\Lambda}_j < 0, \tag{36}$$

$$\lambda_r\widetilde{\Xi}_{jr} + \lambda_j\widetilde{\Xi}_{rj} + (1-\lambda_r)\tilde{\Lambda}_j + (1-\lambda_j)\widetilde{\Lambda}_r < 0, j < r, \tag{37}$$

where

$\widetilde{\Xi}_{jr} = \begin{bmatrix} \widetilde{\Xi}_{jr}^{11} & \widetilde{\Xi}_{jr}^{12} & \widetilde{\Xi}_{jr}^{13} & \widetilde{\Xi}_{jr}^{14} \\ * & \widetilde{\Xi}_{jr}^{22} & \widetilde{\Xi}_{jr}^{23} & \widetilde{\Xi}_{jr}^{24} \\ * & * & \widetilde{\Xi}_{jr}^{33} & \widetilde{\Xi}_{jr}^{34} \\ * & * & * & \widetilde{\Xi}_{jr}^{44} \end{bmatrix}, \widetilde{\Xi}_{jr}^{11} = \begin{bmatrix} \widetilde{\Sigma}_{jr}^{11} & B_{0j}\widetilde{K}_r & \widetilde{R}_1 \\ * & -2\widetilde{R}_2 & \widetilde{R}_2 \\ * & * & \widetilde{\Sigma}^{33} \end{bmatrix}$,

$\widetilde{\Sigma}_{jr}^{11} = A_{0j}\widetilde{P} + \widetilde{P}A_{0j}^{\mathrm{T}} + \widetilde{Q}_1 + \widetilde{Q}_2 - \widetilde{R}_1, \widetilde{\Sigma}^{33} = -\widetilde{Q}_1 - \widetilde{R}_1 - \widetilde{R}_2,$

$\widetilde{\Xi}_{jr}^{12} = \begin{bmatrix} 0 & B_{0j}\widetilde{K}_r & B_{1j} \\ \widetilde{R}_2 & 0 & 0 \\ 0 & 0 & 0 \end{bmatrix}, \widetilde{\Xi}_{jr}^{14} = \begin{bmatrix} E & \varepsilon_1\widetilde{P}G_1^{\mathrm{T}} & 0 \\ 0 & \varepsilon_1\widetilde{K}_r^{\mathrm{T}}G_2^{\mathrm{T}} & \widetilde{P} \\ 0 & 0 & 0 \end{bmatrix},$

$\widetilde{\Xi}_{jr}^{13} = \begin{bmatrix} \tau_m\widetilde{P}A_{0j}^{\mathrm{T}} & \Delta\tau\widetilde{P}A_{0j}^{\mathrm{T}} & \widetilde{P}C^{\mathrm{T}} \\ \tau_m\widetilde{K}_r^{\mathrm{T}}B_{0j}^{\mathrm{T}} & \Delta\tau\widetilde{K}_r^{\mathrm{T}}B_{0j}^{\mathrm{T}} & 0 \\ 0 & 0 & 0 \end{bmatrix},$

$\widetilde{\Xi}^{22} = \mathrm{diag}\left(-\widetilde{Q}_2 - \widetilde{R}_2, -\epsilon_0\left(\kappa_0^2\overline{\Phi} - 2\kappa_0\widetilde{P}\right), -\gamma^2 I\right),$

$\widetilde{\Xi}_{jr}^{23} = \begin{bmatrix} 0 & 0 & 0 \\ \tau_m\widetilde{K}_r^{\mathrm{T}}B_{0j}^{\mathrm{T}} & \Delta\tau\widetilde{K}_r^{\mathrm{T}}B_{0j}^{\mathrm{T}} & 0 \\ \tau_m B_{1j}^{\mathrm{T}} & \Delta\tau B_{1j}^{\mathrm{T}} & 0 \end{bmatrix},$

$\widetilde{\Xi}_{jr}^{24} = \begin{bmatrix} 0 & 0 & 0 \\ 0 & \varepsilon_1\widetilde{K}_r^{\mathrm{T}}G_2^{\mathrm{T}} & \widetilde{P} \\ 0 & 0 & 0 \end{bmatrix}, \widetilde{\Xi}_{jr}^{34} = \begin{bmatrix} \tau_m E_j & 0 & 0 \\ \Delta\tau E_j & 0 & 0 \\ 0 & 0 & 0 \end{bmatrix},$

$\widetilde{\Xi}^{33} = \mathrm{diag}\left(\kappa_1^2\widetilde{R}_1 - 2\kappa_1\widetilde{P}, \kappa_2^2\widetilde{R}_2 - 2\kappa_2\widetilde{P}, -I\right),$

$\widetilde{\Xi}^{44} = \mathrm{diag}\left(-\varepsilon_1 I, -\varepsilon_1 I, -\overline{\Phi}\right).$

In addition, the fuzzy control gains and weight matrix can be determined by $K_r = \widetilde{K}_r\widetilde{P}$, and $\Phi = \overline{\Phi}^{-1}$, respectively.

Proof. By pre- and post-multiplying (32) with $\mathrm{diag}(P^{-1},P^{-1},P^{-1},P^{-1},P^{-1},I,I,I,I,I)$ and letting $\widetilde{P} = P^{-1}$, $\widetilde{Q}_1 = \widetilde{P}Q_1\widetilde{P}$, $\widetilde{Q}_2 = \widetilde{P}Q_2\widetilde{P}$, $\widetilde{R}_1 = \widetilde{P}R_1\widetilde{P}$, $\widetilde{R}_2 = \widetilde{P}R_2\widetilde{P}$, $\widetilde{K}_r = K_r\widetilde{P}$, $\overline{\Phi} = \Phi^{-1}$, we have

$$\begin{bmatrix} \mathfrak{E}_{jr}^{11} & \mathfrak{E}_{jr}^{12} & \mathfrak{E}_{jr}^{13} & \mathfrak{E}_{jr}^{14} \\ * & \mathfrak{E}^{22} & \mathfrak{E}_{jr}^{23} & \mathfrak{E}_{jr}^{24} \\ * & * & \mathfrak{E}^{33} & \mathfrak{E}_{jr}^{34} \\ * & * & * & \mathfrak{E}_{jr}^{44} \end{bmatrix} < 0, \tag{38}$$

where

$\mathfrak{E}_{jr}^{11} = \begin{bmatrix} \widetilde{\Sigma}_{jr}^{11} & B_{0j}\widetilde{K}_r & \widetilde{R}_1 \\ * & \mathfrak{T}^{22} & \widetilde{\Sigma}^{23} \\ * & * & \widetilde{\Sigma}^{33} \end{bmatrix}, \mathfrak{E}_{jr}^{12} = \begin{bmatrix} 0 & B_{0j}\widetilde{K}_r & B_{1j} \\ \widetilde{R}_2 & \widetilde{P}\overline{\Phi}^{-1}\widetilde{P} & 0 \\ 0 & 0 & 0 \end{bmatrix},$

$\mathfrak{E}_{jr}^{13} = \widetilde{\Xi}_{jr}^{13}, \mathfrak{E}_{jr}^{14} = \begin{bmatrix} E_j & \varepsilon_1\widetilde{P}G_1^{\mathrm{T}} \\ 0 & \varepsilon_1\widetilde{K}_r^{\mathrm{T}}G_2^{\mathrm{T}} \\ 0 & 0 \end{bmatrix}, \mathfrak{E}_{jr}^{24} = \begin{bmatrix} 0 & 0 \\ 0 & \varepsilon_1\widetilde{K}_r^{\mathrm{T}}G_2^{\mathrm{T}} \\ 0 & 0 \end{bmatrix},$

$\mathfrak{E}^{22} = \mathrm{diag}\left(-\widetilde{Q}_2 - \widetilde{R}_2, (1-\epsilon_0)\widetilde{P}\overline{\Phi}^{-1}\widetilde{P}, -\gamma^2 I\right),$

$\mathfrak{E}_{jr}^{23} = \widetilde{\Xi}_{jr}^{23}, \mathfrak{E}^{33} = \mathrm{diag}\left(-\widetilde{P}\widetilde{R}_1^{-1}\widetilde{P}, -\widetilde{P}\widetilde{R}_2^{-1}\widetilde{P}, -I\right),$

$\mathfrak{E}_{jr}^{34}=\begin{bmatrix}\tau_m E_j^{\mathrm{T}} & \Delta\tau E_j^{\mathrm{T}} & 0\\ 0 & 0 & 0\end{bmatrix}^{\mathrm{T}}$, $\mathfrak{E}^{44}=\mathrm{diag}\left(-\varepsilon_1 I,-\varepsilon_1 I\right)$,
$\mathfrak{T}^{22}=-2\widetilde{R}_2+\widetilde{P}\overline{\Phi}^{-1}\widetilde{P}$.

Note that $-\widetilde{P}\#^{-1}\widetilde{P}$ are nonlinear terms, where $\#$ stands for $\widetilde{R}_1$ and $\widetilde{R}_2$, respectively. From **Lemma 3**, those nonlinear terms can be replaced with $\kappa_k^2\#-2\kappa_k\widetilde{P}\,(k=1,2)$. It is then not difficult to derive $\widetilde{\Xi}_{jr}$ in (35) from (38) by using the Schur complement and **Lemma 3** to deal with the nonlinear term $-\widetilde{P}\overline{\Phi}^{-1}\widetilde{P}$. This completes the proof. ■

Remark 10. For CETCM, only the matrix $\Phi>0$ is required [19], [23]. In this case, let $\widetilde{\Phi}\triangleq\widetilde{P}\overline{\Phi}^{-1}\widetilde{P}$, then weight matrix Φ with the CETCM is given by $\Phi=\widetilde{P}^{-1}\widetilde{\Phi}\widetilde{P}^{-1}$, where $\widetilde{\Phi}$ and $\widetilde{P}$ can be obtained by solving (38). However, for DETCM, since the block diagonal structure of Φ cannot be guaranteed, the above variable substitution method is not applicable. From linear algebra, the inverse of a block diagonal matrix, if it exists, is also a block diagonal matrix. Given this, denote $\overline{\Phi}\triangleq\Phi^{-1}$ and $\widetilde{P}\triangleq P^{-1}$, then one has $\widetilde{P}\Phi\widetilde{P}=\widetilde{P}\overline{\Phi}^{-1}\widetilde{P}$. On this basis, using the Schur complement and **Lemma 3**, $\overline{\Phi}$ can be solved directly according to **Theorem 2**, thereby ensuring the block diagonal structure of matrix Φ.

In general, it is desired that the H_∞ performance index γ is as small as possible. In this case, its minimum value can be obtained by the following corollary.

Corollary 1. *The minimum H_∞ performance γ^* in **Theorem 2** can be found by solving the following convex optimization problem:*

$$\gamma^*=\min\ \gamma$$

$$\text{s.t. (35), (36), } \textit{and} \text{ (37).}$$

It is necessary mention that the slack matrix introduced in **Theorem 2** provides more design flexibility, thereby alleviating the conservatism of the results. If the slack matrix is not introduced, we have the following corollary.

Corollary 2. *For the given constants γ, h, ϵ_0, τ_m, τ_M $(0<\tau_m\le\tau_M)$, and the membership functions satisfying $\mu_r-\lambda_r\eta_r>0$ $(0<\lambda_r\le 1)$, closed-loop system (24) is asymptotically stable with control gains K_r if there exist symmetric positive definite matrices $\widetilde{P}$, $\widetilde{\Phi}$, $\widetilde{Q}_1$, $\widetilde{Q}_2$, $\widetilde{R}_1$, and $\widetilde{R}_2$ of appropriate dimensions such that the following linear matrix inequality conditions hold for any $j,r=1,2,\ldots,8$:*

$$\widetilde{\Xi}_{jr}<0, \tag{39}$$

$$\lambda_j\widetilde{\Xi}_{jj}<0, \tag{40}$$

$$\lambda_r\widetilde{\Xi}_{jr}+\lambda_j\widetilde{\Xi}_{rj}<0, j<r. \tag{41}$$

Similar to **Corollary 1**, we can achieve the following corollary.

Corollary 3. *The minimum H_∞ performance γ^* in **Corollary 2** can be obtained by solving the following convex optimization problem:*

$$\gamma^*=\min\ \gamma$$

$$\text{s.t. (39), (40), } \textit{and} \text{ (41).}$$

IV. Numerical simulation

This section validates the effectiveness of the proposed method with numerical simulation.

A. Simulation settings

Two simulation cases, i.e., the double-lane change and lane change maneuvers, are constructed in the CarSim-Simulink joint-simulation environment. Furthermore, a CAN model is built through Simulink/SimEvents, which is composed of one bus model and three network node models, and those who are interested can refer to [49] for details. An E-Class SUV in CarSim is selected as the controlled AGV, and its normal parameters are listed in Table II.

In this study, the sampling interval of sensors is 0.01s, and the minimum and maximum CAN-induced delay are $\tau_m=0.001$s, and $\tau_M=0.02$s, respectively. Because of this communication delay, the membership factors μ_r and η_r will depend on different premise variables, as discussed in Section II-C. Considering that the vehicle mass won't change in a short period, to simplify the problem, we set the vehicle mass to its nominal value m_0 when determining the value of λ_r. In order to ensure membership function design condition $\mu_r-\lambda_r\eta_r>0$ always holds, as we can see from (10) and (23), the main factor that affects λ_r is the change in vehicle speed, i.e., longitudinal acceleration a_x. For convenience, we call λ_r the membership function parameter. To determine the value of the membership function parameter, we examine some typical vehicle test cycles, such as NEDC, UDDS, and WLTC, whose velocity and acceleration profiles are shown in Fig. 3. There is no doubt that the acceleration of the above vehicle test cycles is bounded, and the supre- and infimum accelerations are denoted by a_{xsup} and a_{xinf}, respectively. Therefore, the speed change due to communication delay is also bounded, and we have that

$$\overline{\Delta v_x}=\mathcal{F}\cdot\tau_M\cdot a_{xsup}\ ,\quad \underline{\Delta v_x}=\mathcal{F}\cdot\tau_M\cdot a_{xinf}, \tag{42}$$

where $\mathcal{F}$ is the scale factor. Then we can use Algorithm 1 to determine λ_r.

In the simulation, the uncertain cornering stiffness is assumed to be 10% of the normal value. For given scalars $\epsilon_0=100$, $\kappa_0=0.2$, $\kappa_1=0.15$, $\kappa_2=0.1$, and λ_r, the corresponding control gains K_r and matrix Φ can be obtained by using **Corollary 1** and the YALMIP toolbox [50]. Furthermore, the minimal γ obtained is 92.25, which is smaller than the minimal γ obtained by **Corollary 3** of 94.34.

To highlight the performance of the proposed DETCM-based fuzzy feedback controller, a decentralized time-triggered communication mechanism (DTTCM) based controller is used for comparison, which can be derived from (11) by letting $\epsilon_n(t)=0$. The following transmission rate (TR) is adopted as a performance metric of communication efficiency

$$\mathrm{TR}=\frac{N_1}{N_2}\cdot 100\%, \tag{43}$$

where N_1 denotes the number of transmitted sample signals released by the relevant event generator, and N_2 represents the total number of sampled signals, respectively.

Algorithm 1 Determine the value of the membership function parameter λ_r.

Input: $\overline{\Delta v_x}$, $\underline{\Delta v_x}$, $\overline{v}_x$, $\underline{v}_x$, $\overline{m}$, $\underline{m}$, m_0
Output: λ_r

function H ($\sigma, \overline{\sigma}, \underline{\sigma}$)
  if $\sigma > \overline{\sigma}$ **then** $\sigma = \overline{\sigma}$ **end if**
  if $\sigma < \underline{\sigma}$ **then** $\sigma = \underline{\sigma}$ **end if**
  $H_1(\sigma) = (\overline{\sigma} - \sigma)/(\overline{\sigma} - \underline{\sigma})$, $H_2(\sigma) = 1 - H_1(\sigma)$
  return H_1, H_2
end function
function M $(H_{1,1}, H_{1,2}, H_{2,1}, H_{2,2}, H_{3,1}, H_{3,2})$
  Calculate $\eta_1 \sim \eta_8$ according to (10)
  return $\eta_1 \sim \eta_8$
end function

$\lambda_r = \text{ones}(1, 8)$, $H_{3,1}, H_{3,2} \leftarrow$ H $(\frac{1}{m_0}, \frac{1}{\underline{m}}, \frac{1}{\overline{m}})$
for $v_x = \underline{v}_x : dv_x : \overline{v}_x$ **do**
  $H_{1,1}, H_{1,2} \leftarrow$ H $(v_x, \overline{v}_x, \underline{v}_x)$
  $H_{2,1}, H_{2,2} \leftarrow$ H $(\frac{1}{v_x}, \frac{1}{\underline{v}_x}, \frac{1}{\overline{v}_x})$
  $\eta_1 \sim \eta_8 \leftarrow$ M $(H_{1,1}, H_{1,2}, H_{2,1}, H_{2,2}, H_{3,1}, H_{3,2})$
  for $v'_x = v_x + \underline{\Delta v_x} : \delta v_x : v_x + \overline{\Delta v_x}$ **do**
    $H'_{1,1}, H'_{1,2} \leftarrow$ H $(v'_x, \overline{v}_x, \underline{v}_x)$
    $H'_{2,1}, H'_{2,2} \leftarrow$ H $(\frac{1}{v'_x}, \frac{1}{\underline{v}_x}, \frac{1}{\overline{v}_x})$
    $\eta'_1 \sim \eta'_8 \leftarrow$ M $(H'_{1,1}, H'_{1,2}, H'_{2,1}, H'_{2,2}, H_{3,1}, H_{3,2})$
    for $i = 1 : 1 : 2^3$ **do**
      $\lambda_r(i) = \min[\lambda_r(i), \text{floor}(100 \cdot \eta_i/\eta'_i)/100)]$
    end for
  end for
end for

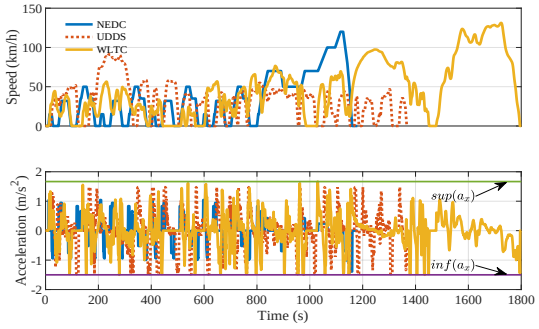

Fig. 3. Velocity and acceleration profiles for NEDC, UDDS, and WLTC vehicle test cycles.

B. Scenario A: double-lane change maneuver

In this subsection, the double-lane change maneuver is performed to verify the controller performance. The reference trajectory, road curvature, and longitudinal velocity of the vehicle model are shown in Fig. 4. A PI controller is adopted to regulate the actual longitudinal vehicle velocity to track the reference.

Simulation results with two different triggering mechanisms, i.e., DTTCM and DETCM, are shown in Fig. 5. It is observed that the path tracking performance, in terms of lateral offset and heading error, are almost the same for both mechanisms. At the same time, the two triggering mechanisms can also produce similar lateral velocity and yaw rate, as depicted in Fig. 6. To compare the path tracking performance with different triggering mechanisms, the statistical metrics in the simulation process, namely, the root mean square (RMS) and maximum (MAX) value of lateral offset and heading

TABLE II
NORMAL VALUE IN SIMULATION

m	I_z	v_x	C_{0f}	C_{0r}	a/b
$[1702, 1881]$ kg	$[2491, 2754]$ kg $\cdot$ m^2	$[36, 54]$ km/h	41877 N/rad	47149 N/rad	1.39/1.56 m

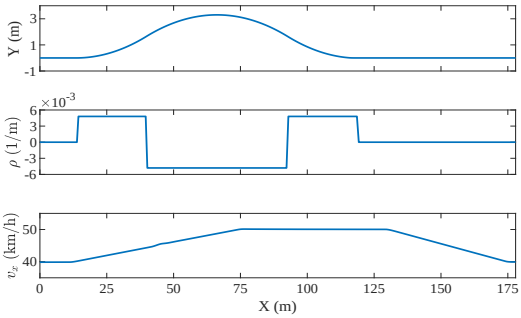

Fig. 4. Reference trajectory, road curvature, and longitudinal vehicle velocity in Scenario A, where the road curvature is within $[-4.8, 4.8] \cdot 10^{-3}\text{m}^{-1}$, and the longitudinal vehicle velocity ranges within $[40, 50]\text{km/h}$.

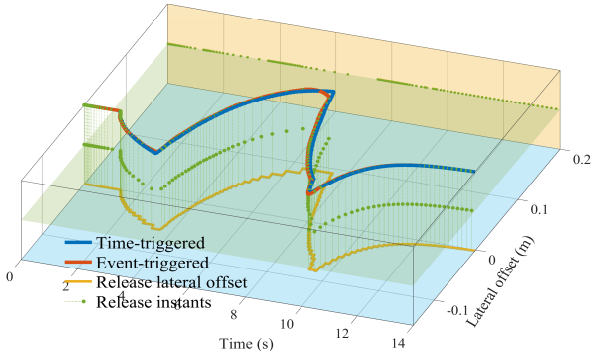

(a) Lateral offset

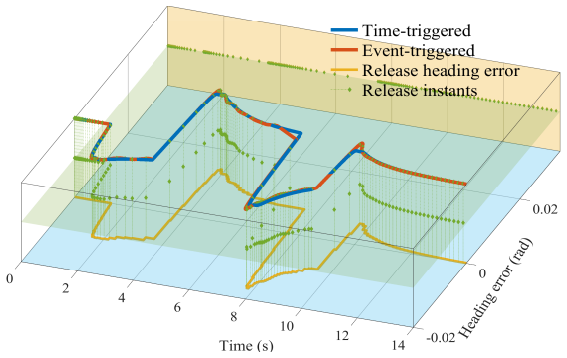

(b) Heading error

Fig. 5. Results in Scenario A. The blue and red solid curves represent the path following errors with DTTCM and DETCM, respectively. The orange stairstep curves show the release values of lateral offset and heading error that satisfy the relevant triggering conditions, and the release moments are marked with green solid circles and diamonds, respectively.

TABLE III
COMPARISON OF PATH TRACKING PERFORMANCE WITH DTTCM AND DETCM

Scenario A	Lateral offset (m)		Heading error (rad)	
	RMS	MAX	RMS	MAX
DTTCM	0.0473	0.0973	0.0075	0.0159
DETCM	0.0473	0.0950	0.0074	0.0170
Scenario B	**Lateral offset (m)**		**Heading error (rad)**	
	RMS	MAX	RMS	MAX
DTTCM	0.0383	0.0892	0.0077	0.0167
DETCM	0.0382	0.0917	0.0078	0.0185

TABLE IV
TR FOR EACH NETWORK NODE WITH DETCM

	Scenario A			Scenario B		
	e_y & e_ψ	v_y	r	e_y & e_ψ	v_y	r
Release times	124	121	111	105	168	128
TR(%)	8.9	8.7	8.0	10.5	16.8	12.8
↑ (%)	91.1	91.3	92.0	89.5	83.2	87.2

error, are shown in Table III. As we can see, these two triggering mechanisms are capable of achieving similar path tracking results and maintaining maximum lateral and heading deviations within small ranges, which are about $0.10\mathrm{m}$ for lateral offset and $0.02\mathrm{rad}$ for heading error.

To evaluate the communication performance of DETCM, the release instant of each sensor is highlighted with corresponding symbols in Fig. 5 and Fig. 6, from which it can be seen that the data transmission of sensors exhibits obvious sparse features. Further evaluation results, including the number of sampling data released by the event generator, TR and performance improvement, are illustrated in Table IV. It can be seen that the number of release data per sensor with DETCM is 124, 121, and 111 times, respectively, while DTTCM is 1400 times for each sensor. This indicates that DETCM greatly saves bandwidth resources by transmitting much less sampled data.

By projecting the sensor release values, i.e., the value received by the controller, onto the bottom horizontal plane, it can be seen that the previous release value will remain unchanged until a new one is received. By using these received release values, the control input, i.e., front wheel steering angle, can be obtained, which shows obvious step changes with slight jitter due to the event-triggered mechanism. The front wheel steering angle and the corresponding global trajectories of the AGV are shown in Fig. 7.

C. Scenario B: lane change maneuver

In the simulation, the AGV is supposed to complete a lane change maneuver at varying longitudinal velocities. Fig. 8 exhibits the reference trajectory, path curvature, and longitudinal velocity profile of the AGV in Scenario B.

Fig. 9 shows the results for lateral offset and heading error, indicating that DETCM can achieve a comparable path tracking performance with a much lower release frequency than DTTCM. As shown in Table III, both mechanisms guarantee

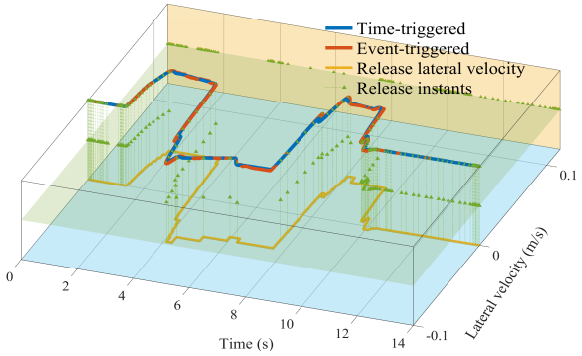

(a) Lateral velocity

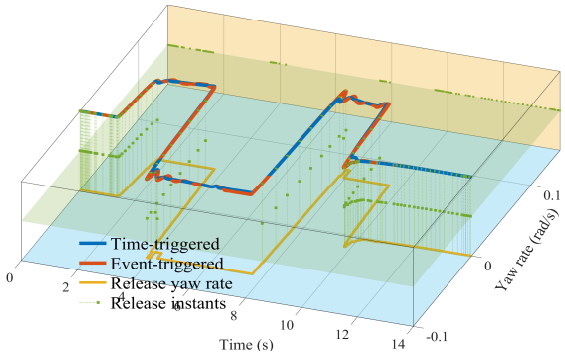

(b) Yaw rate

Fig. 6. Results in Scenario A. The blue and red solid curves represent the lateral vehicle dynamic of the AGV with DTTCM and DETCM, respectively. The orange stairstep curves show the release values of lateral velocity and yaw rate that satisfy the relevant triggering conditions, and the release moments are marked with green solid triangles and squares, respectively.

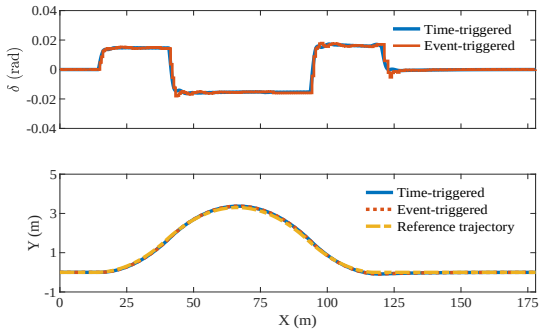

Fig. 7. The front wheel steering angle and global trajectories of the AGV in Scenario A.

that path tracking deviations are within the safe region [19] and have similar statistical properties when comparing the RMS and maximum values of lateral and heading deviations for event-triggering and time-triggering cases. Furthermore, as illustrated in Fig. 10, the vehicle's lateral dynamics, such as its lateral velocity and yaw rate, also exhibit similar characteristics.

In addition, DETCM has obvious advantages in release frequency, as shown in Table IV, while guaranteeing satisfactory path tracking performance. The results shows that, on average, TR is only 13.4% with DETCM compared to DTTCM. The above results further verify the effectiveness of the proposed DETCM in saving communication resources. Finally, the

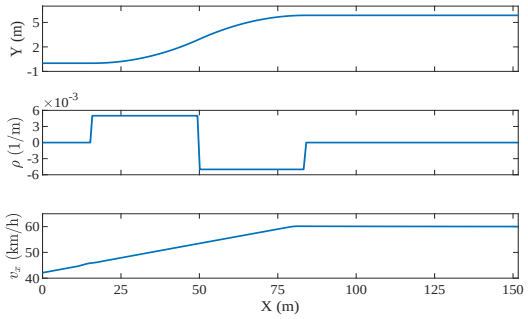

Fig. 8. Reference trajectory, road curvature, and longitudinal vehicle velocity in Scenario B, where the road curvature is within $[-0.005, 0.005]\mathrm{m}^{-1}$, and the longitudinal vehicle velocity varies within $[40, 60]\mathrm{km/h}$.

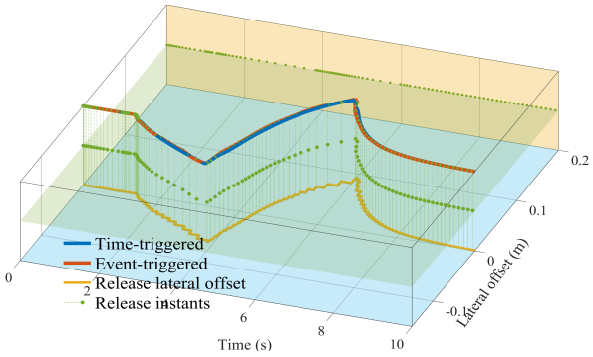

(a) Lateral offset

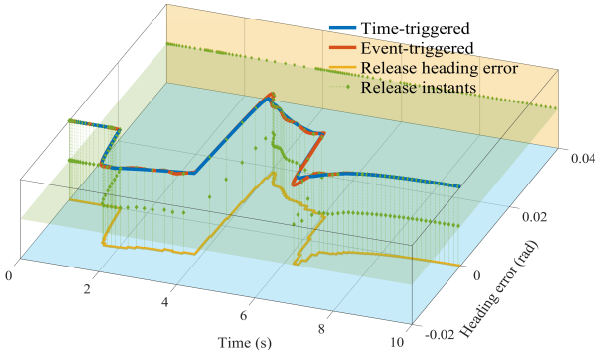

(b) Heading error

Fig. 9. Results in Scenario B. The blue and red solid curves represent the path following errors with DTTCM and DETCM, respectively. The orange stairstep curves show the release values of lateral offset and heading error that satisfy the relevant triggering conditions, and the release moments are marked with green solid circles and diamonds, respectively.

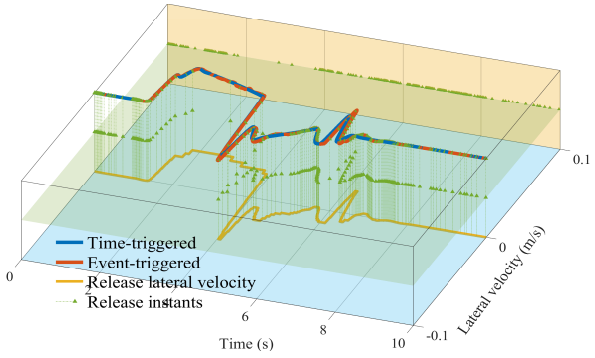

(a) Lateral velocity

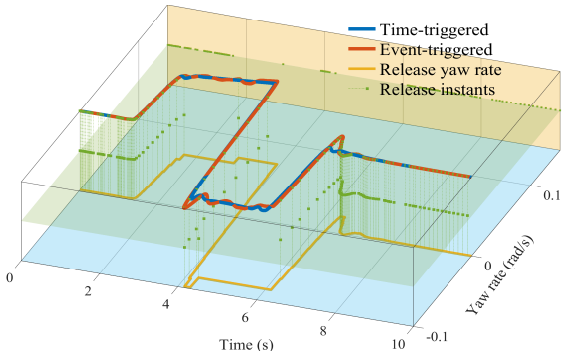

(b) Yaw rate

Fig. 10. Results in Scenario B. The blue and red solid curves represent the lateral vehicle dynamic of the AGV with DTTCM and DETCM, respectively. The orange stairstep curves show the release values of lateral velocity and yaw rate that satisfy the relevant triggering conditions, and the release moments are marked with green solid triangles and squares, respectively.

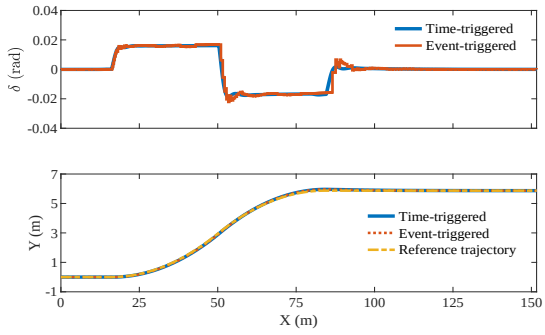

Fig. 11. The front wheel steering angle and global trajectories of the AGV in Scenario B.

global trajectory of the AGV and the corresponding control inputs are shown in Fig. 11. It can be seen that both triggering mechanisms can track the reference trajectory well.

V. Conclusion

This paper has investigated the joint design problem of decentralized event-triggered communication and a path tracking control algorithm for AGVs. A general T-S fuzzy model considering norm bounded time-varying parameters has been derived. To reduce unnecessary data transfer between the sensors and the controller, a DETCM has been proposed. Furthermore, a co-design method is proposed for decentralized event-triggered communication scheduling and IPM-based path tracking control. Simulations have demonstrated that the proposed scheme can guarantee reliable path tracking performance and reduce communication occupancy by an average of 91.5% and 88.6% in two typical scenarios, respectively, compared with the DTTCM strategy.

Our future goal is to design a path tracking controller that uses observer- or output-based feedback. In addition, the impact of measurement noise on path tracking performance during practical implementation is also worthy of further study.

REFERENCES

[1] X. Li, Z. Sun, D. Cao, D. Liu, and H. He, "Development of a new integrated local trajectory planning and tracking control framework for autonomous ground vehicles," *Mechanical Systems and Signal Processing*, vol. 87, pp. 118–137, 2017.

[2] S. Cheng, L. Li, X. Chen, J. Wu, and H.-d. Wang, "Model-predictive-control-based path tracking controller of autonomous vehicle considering parametric uncertainties and velocity-varying," *IEEE Transactions on Industrial Electronics*, vol. 68, no. 9, pp. 8698–8707, 2021.

[3] B. Paden, M. Čáp, S. Z. Yong, D. Yershov, and E. Frazzoli, "A survey of motion planning and control techniques for self-driving urban vehicles," *IEEE Transactions on Intelligent Vehicles*, vol. 1, no. 1, pp. 33–55, 2016.

[4] M. Hu, C. Li, Y. Bian, H. Zhang, Z. Qin, and B. Xu, "Fuel economy-oriented vehicle platoon control using economic model predictive control," *IEEE Transactions on Intelligent Transportation Systems*, vol. 23, no. 11, pp. 20 836–20 849, 2022.

[5] S. Xu and H. Peng, "Design, analysis, and experiments of preview path tracking control for autonomous vehicles," *IEEE Transactions on Intelligent Transportation Systems*, vol. 21, no. 1, pp. 48–58, 2020.

[6] Y. Wang, H. Ding, J. Yuan, and H. Chen, "Output-feedback triple-step coordinated control for path following of autonomous ground vehicles," *Mechanical Systems and Signal Processing*, vol. 116, pp. 146–159, 2019.

[7] Z. Yang, J. Huang, D. Yang, and Z. Zhong, "Design and optimization of robust path tracking control for autonomous vehicles with fuzzy uncertainty," *IEEE Transactions on Fuzzy Systems*, vol. 30, no. 6, pp. 1788–1800, 2022.

[8] Z. Hu, J. Huang, Z. Yang, and Z. Zhong, "Cooperative-game-theoretic optimal robust path tracking control for autonomous vehicles," *Journal of Vibration and Control*, vol. 28, no. 5-6, pp. 520–535, 2022.

[9] Q. An, S. Cheng, C. Li, L. Li, and H. Peng, "Game theory-based control strategy for trajectory following of four-wheel independently actuated autonomous vehicles," *IEEE Transactions on Vehicular Technology*, vol. 70, no. 3, pp. 2196–2208, 2021.

[10] S. Milani, H. Khayyam, H. Marzbani, W. Melek, N. L. Azad, and R. N. Jazar, "Smart autodriver algorithm for real-time autonomous vehicle trajectory control," *IEEE Transactions on Intelligent Transportation Systems*, vol. 23, no. 3, pp. 1984–1995, 2022.

[11] J. Chen, Z. Shuai, H. Zhang, and W. Zhao, "Path following control of autonomous four-wheel-independent-drive electric vehicles via second-order sliding mode and nonlinear disturbance observer techniques," *IEEE Transactions on Industrial Electronics*, vol. 68, no. 3, pp. 2460–2469, 2021.

[12] G. Chen, J. Yao, H. Hu, Z. Gao, L. He, and X. Zheng, "Design and experimental evaluation of an efficient MPC-based lateral motion controller considering path preview for autonomous vehicles," *Control Engineering Practice*, vol. 123, p. 105164, 2022.

[13] S. Mata, A. Zubizarreta, and C. Pinto, "Robust tube-based model predictive control for lateral path tracking," *IEEE Transactions on Intelligent Vehicles*, vol. 4, no. 4, pp. 569–577, 2019.

[14] H. Guo, D. Cao, H. Chen, Z. Sun, and Y. Hu, "Model predictive path following control for autonomous cars considering a measurable disturbance: Implementation, testing, and verification," *Mechanical Systems and Signal Processing*, vol. 118, pp. 41–60, 2019.

[15] J. Ji, A. Khajepour, W. W. Melek, and Y. Huang, "Path planning and tracking for vehicle collision avoidance based on model predictive control with multiconstraints," *IEEE Transactions on Vehicular Technology*, vol. 66, no. 2, pp. 952–964, 2017.

[16] A.-T. Nguyen, C. Sentouh, H. Zhang, and J.-C. Popieul, "Fuzzy static output feedback control for path following of autonomous vehicles with transient performance improvements," *IEEE Transactions on Intelligent Transportation Systems*, vol. 21, no. 7, pp. 3069–3079, 2020.

[17] C. Zhang, J. Hu, J. Qiu, W. Yang, H. Sun, and Q. Chen, "A novel fuzzy observer-based steering control approach for path tracking in autonomous vehicles," *IEEE Transactions on Fuzzy Systems*, vol. 27, no. 2, pp. 278–290, 2019.

[18] L. Zhang, Y. Wu, B. Li, B. Zhang, and N. Zhang, "A novel manoeuvre stability controller based on vehicle state prediction and intellectual braking torque distribution," *Proceedings of the Institution of Mechanical Engineers, Part D: Journal of Automobile Engineering*, vol. 234, no. 1, pp. 136–151, 2020.

[19] J. Zhang, B. Zhang, N. Zhang, C. Wang, and Y. Chen, "A novel robust event-triggered fault tolerant automatic steering control approach of autonomous land vehicles under in-vehicle network delay," *International Journal of Robust and Nonlinear Control*, vol. 31, no. 7, pp. 2436–2464, 2021.

[20] P. Li, P. Li, J. Zhao, and B. Zhang, "Robust gain-scheduling static output-feedback H_∞ control of vehicle lateral stability with heuristic approach," *Information Sciences*, vol. 546, pp. 220–233, 2021.

[21] S. Zhu, S. Y. Gelbal, B. Aksun-Guvenc, and L. Guvenc, "Parameter-space based robust gain-scheduling design of automated vehicle lateral control," *IEEE Transactions on Vehicular Technology*, vol. 68, no. 10, pp. 9660–9671, 2019.

[22] M. Corno, G. Panzani, F. Roselli, M. Giorelli, D. Azzolini, and S. M. Savaresi, "An LPV approach to autonomous vehicle path tracking in the presence of steering actuation nonlinearities," *IEEE Transactions on Control Systems Technology*, vol. 29, no. 4, pp. 1766–1774, 2021.

[23] W. Li, Z. Xie, J. Zhao, and P. K. Wong, "Velocity-based robust fault tolerant automatic steering control of autonomous ground vehicles via adaptive event triggered network communication," *Mechanical Systems and Signal Processing*, vol. 143, p. 106798, 2020.

[24] Z. Yang, J. Huang, H. Yin, D. Yang, and Z. Zhong, "Path tracking control for underactuated vehicles with matched-mismatched uncertainties: An uncertainty decomposition based constraint-following approach," *IEEE Transactions on Intelligent Transportation Systems*, vol. 23, no. 8, pp. 12 894–12 907, 2022.

[25] M. Di Natale and A. L. Sangiovanni-Vincentelli, "Moving from federated to integrated architectures in automotive: The role of standards, methods and tools," *Proceedings of the IEEE*, vol. 98, no. 4, pp. 603–620, 2010.

[26] F. Li, J. Fu, and D. Du, "An improved event-triggered communication mechanism and L_∞ control co-design for network control systems," *Information Sciences*, vol. 370, pp. 743–762, 2016.

[27] D. Yue, E. Tian, and Q.-L. Han, "A delay system method for designing event-triggered controllers of networked control systems," *IEEE Transactions on Automatic Control*, vol. 58, no. 2, pp. 475–481, 2012.

[28] Z. Gao, D. Zhang, S. Zhu, and J.-e. Feng, "Distributed active disturbance rejection control for ackermann steering of a four-in-wheel motor drive vehicle with deception attacks on controller area networks," *Information Sciences*, vol. 540, pp. 370–389, 2020.

[29] I. Ahmad, X. Ge, and Q.-L. Han, "Decentralized dynamic event-triggered communication and active suspension control of in-wheel motor driven electric vehicles with dynamic damping," *IEEE/CAA Journal of Automatica Sinica*, vol. 8, no. 5, pp. 971–986, 2021.

[30] Z. Qi, Q. Shi, and H. Zhang, "Tuning of digital PID controllers using particle swarm optimization algorithm for a CAN-based DC motor subject to stochastic delays," *IEEE Transactions on Industrial Electronics*, vol. 67, no. 7, pp. 5637–5646, 2020.

[31] R. Wang, H. Jing, C. Hu, F. Yan, and N. Chen, "Robust H_∞ path following control for autonomous ground vehicles with delay and data dropout," *IEEE Transactions on Intelligent Transportation Systems*, vol. 17, no. 7, pp. 2042–2050, 2016.

[32] Q. Shi and H. Zhang, "Road-curvature-range-dependent path following controller design for autonomous ground vehicles subject to stochastic delays," *IEEE Transactions on Intelligent Transportation Systems*, vol. 23, no. 10, pp. 17 440–17 450, 2022.

[33] Z. Luan, J. Zhang, W. Zhao, and C. Wang, "Trajectory tracking control of autonomous vehicle with random network delay," *IEEE Transactions on Vehicular Technology*, vol. 69, no. 8, pp. 8140–8150, 2020.

[34] C. Peng and F. Li, "A survey on recent advances in event-triggered communication and control," *Information Sciences*, vol. 457, pp. 113–125, 2018.

[35] X. Ge, I. Ahmad, Q.-L. Han, J. Wang, and X.-M. Zhang, "Dynamic event-triggered scheduling and control for vehicle active suspension over controller area network," *Mechanical Systems and Signal Processing*, vol. 152, p. 107481, 2021.

[36] W. Li, Z. Xie, P. K. Wong, X. Mei, and J. Zhao, "Adaptive-event-trigger-based fuzzy nonlinear lateral dynamic control for autonomous electric vehicles under insecure communication networks," *IEEE Transactions on Industrial Electronics*, vol. 68, no. 3, pp. 2447–2459, 2021.

[37] H. Zhang, Q. Hong, H. Yan, and Y. Luo, "Observer-based decentralized event-triggered H_∞ control for networked systems," *Journal of the Franklin Institute*, vol. 354, no. 9, pp. 3744–3759, 2017.

[38] P. Tallapragada and N. Chopra, "Decentralized event-triggering for control of nonlinear systems," *IEEE Transactions on Automatic Control*, vol. 59, no. 12, pp. 3312–3324, 2014.

[39] G. Zhao, C. Hua, and X. Guan, "Decentralized dynamic event-triggered $\mathcal{H}_\infty$ control for nonlinear systems with unreliable communication channel and limited bandwidth," *IEEE Transactions on Fuzzy Systems*, vol. 29, no. 4, pp. 757–771, 2021.

[40] H. K. Lam and M. Narimani, "Stability analysis and performance design for fuzzy-model-based control system under imperfect premise

matching," *IEEE Transactions on Fuzzy Systems*, vol. 17, no. 4, pp. 949–961, 2009.
[41] C. Peng, S. Ma, and X. Xie, "Observer-based Non-PDC control for networked T–S fuzzy systems with an event-triggered communication," *IEEE Transactions on Cybernetics*, vol. 47, no. 8, pp. 2279–2287, 2017.
[42] H. Zhang, X. Zhang, and J. Wang, "Robust gain-scheduling energy-to-peak control of vehicle lateral dynamics stabilisation," *Vehicle System Dynamics*, vol. 52, no. 3, pp. 309–340, 2014.
[43] P. Li, A.-T. Nguyen, H. Du, Y. Wang, and H. Zhang, "Polytopic LPV approaches for intelligent automotive systems: State of the art and future challenges," *Mechanical Systems and Signal Processing*, vol. 161, p. 107931, 2021.
[44] H. O. Wang and K. Tanaka, *Fuzzy control systems design and analysis: A linear matrix inequality approach*. John Wiley & Sons, 2004.
[45] Z. Qin, L. Chen, M. Hu, and X. Chen, "A Lateral and Longitudinal Dynamics Control Framework of Autonomous Vehicles Based on Multi-Parameter Joint Estimation," *IEEE Transactions on Vehicular Technology*, vol. 71, no. 6, pp. 5837–5852, 2022.
[46] D. Zhang, C. Lv, T. Yang, and P. Hang, "Cyber-Attack Detection for Autonomous Driving Using Vehicle Dynamic State Estimation," *Automotive Innovation*, vol. 4, no. 3, pp. 262–273, 2021.
[47] L. Zhang, B. Li, H. Du, and B. Zhang, "Takagi-Sugeno Fuzzy-based Kalman Filter Observer for Vehicle Side-slip Angle Estimation and Lateral Stability Control," in *2019 3rd International Symposium on Autonomous Systems (ISAS)*. Shanghai, China: IEEE, 2019, pp. 352–357.
[48] X. Jiang and Q.-L. Han, "Delay-dependent robust stability for uncertain linear systems with interval time-varying delay," *Automatica*, vol. 42, no. 6, pp. 1059–1065, 2006.
[49] Effects of communication delays on an ABS control system - MATLAB & Simulink. [Online]. Available: https://www.mathworks.com/help/simevents/ug/effects-of-communication-delays-on-an-abs-control-system.html
[50] J. Lofberg, "Yalmip: A toolbox for modeling and optimization in MATLAB," in *2004 IEEE international conference on robotics and automation (IEEE Cat. No. 04CH37508)*. IEEE, 2004, pp. 284–289.

Liqin Zhang received the B.E. degree from Chang'an University, Xi'an, China, in 2016, and the M.S. degree from the Hunan University, Changsha, China, in 2019. He is currently pursuing the Ph.D. degree in mechanical engineering with Hunan University, Changsha, China.

His current research interests include vehicle dynamics and control, networked control systems, and their applications to autonomous vehicles.

Manjiang Hu received the B.Tech. and Ph.D. degrees from Jiangsu University, Zhenjiang, China, in 2009 and 2014, respectively.

He held a post-doctoral position at the Department of Automotive Engineering, Tsinghua University, Beijing, China, from 2014 to 2017. He is currently a Professor with the College of Mechanical and Vehicle Engineering, Hunan University, Changsha, China. His research interests include cooperative driving assistance technology and vehicle control.

Hui Zhang (Senior Member, IEEE) received the B.Sc. degree in mechanical design manufacturing and automation from the Harbin Institute of Technology at Weihai, Weihai, China, in 2006, the M.Sc. degree in automotive engineering from Jilin University, Changchun, China, in 2008, and the Ph.D. degree in mechanical engineering from the University of Victoria, Victoria, BC, Canada, in 2012.

Dr. Zhang is also a member of the SAE International and American Society of Mechanical Engineers (ASME). He also serves as a Board Member of International Journal of Electric and Hybrid Vehicles, Mechanical Systems, and Signal Processing. He was a recipient of the 2017 IEEE Transactions on Fuzzy Systems Outstanding Paper Award, the 2018 SAE Ralph R. Teetor Educational Award, the IEEE Vehicular Technology Society 2019 Best Vehicular Electronics Paper Award, and the 2019 SAE International Intelligent and Connected Vehicles Symposium Best Paper Award. He also serves as an Associate Editor for IEEE Transactions on Intelligent Vehicles, The Journal of the Franklin Institute, SAE International Journal of Connected and Automated Vehicles, IEEE Open Journal of the Industrial Electronics Society, and ASME Transactions Journal of Dynamic Systems, Measurement and Control.

Yougang Bian (Member, IEEE) received the B.E. and Ph.D. degrees from Tsinghua University, Beijing, China, in 2014 and 2019, respectively.

He was a Visiting Scholar with the Department of Electrical and Computer Engineering, University of California at Riverside, Riverside, CA, USA, from 2017 to 2018. His research interests include distributed control, cooperative control, and their applications to connected and automated vehicles.

Dr. Bian was a recipient of the Best Paper Award at the 2017 IEEE Intelligent Vehicles Symposium.

Anh-Tu Nguyen (Member, IEEE) received the degree in engineering and the M.Sc. degree in automatic control from the Grenoble Institute of Technology, France, in 2009, and the Ph.D. degree in automatic control from the Université Polytechnique Hauts-de-France, Valenciennes, France, in 2013.

In 2010, after working for a short period at the French Institute of Petroleum, Rueil-Malmaison, France, he began his doctoral program at the University of Valenciennes, France, in collaboration with the VALEO Group. From 2014 to 2018, he was a Post-Doctoral Researcher with the laboratory LAMIH UMR CNRS 8201, Valenciennes, France, and the laboratory LS2N UMR CNRS 6004, Nantes, France. He is currently an Associate Professor with the Université Polytechnique des Hauts-de-France, Valenciennes. His research interests include robust control and estimation, constrained control, and human–machine shared control for intelligent vehicles.

Rongjun Ding received the B.S. degree from Southwest Jiaotong University, Sichuan, China, in 1984, and the Ph.D. degree from Central South University, Changsha, China, in 2008.

He is currently a Professor with Hunan University, Changsha, China. He was an Elected Member of the Chinese Academy of Engineering in 2011. His research interest includes AC dive systems for electric locomotives and intelligent control of vehicles.